Front Delineation and Tracking with Multiple Underwater Vehicles

Andrew Branch[1], Mar M. Flexas[2], Brian Claus[3], Andrew F. Thompson[2], Evan B. Clark[1], Yanwu Zhang[4], James C. Kinsey[3], Steve Chien[1], David M. Fratantoni[5], Brett Hobson[4], Brian Kieft[4], Francisco P. Chavez[4]

[1]Jet Propulsion Laboratory, California Institute of Technology
[2]California Institute of Technology
[3]Woods Hole Oceanographic Institution
[4]Monterey Bay Aquarium Research Institute
[5]Remote Sensing Solutions
Correspondence Author: andrew.branch@jpl.nasa.gov

Abstract

This work describes a method for detecting and tracking ocean fronts using multiple autonomous underwater vehicles. Multiple vehicles — equally-spaced along the expected frontal boundary — complete near parallel transects orthogonal to the front. Lateral gradients are used to determine the location of the front crossing from each individual vehicle transect by detecting a change in the observed water property. Adaptive control of the vehicles ensure they remain perpendicular to the estimated front boundary as it evolves over time. This method was demonstrated in and around Monterey Bay, California in May of 2017. We compare the front detection method to previously used methods. We introduce a metric in order to evaluate the adaptive control techniques presented. We show the capability of this method for repeated sampling across a dynamic two-dimensional ocean front using short-range Iver AUVs. This method extends to tracking gradients of different properties using a variety of vehicles.

Introduction

Space-based remote sensing can provide extensive information about ocean dynamics. However, remote sensing information is generally limited to measuring the ocean surface. To probe the ocean interior efficiently requires marine vehicles such as autonomous underwater vehicles (AUVs), gliders, profiling buoys, surface vehicles, and ships sampling in situ. Unfortunately, building, deploying and operating these in situ marine robotic explorers is expensive. As a result, any actual study involves a limited number of marine vehicles, especially when compared to the vast expanse of the ocean. Determining where to deploy and operate marine assets is a challenging problem given the 4D spatiotemporal variations in oceanographic phenomena.

The use of autonomous marine vehicles will increase as the size of ocean observing systems expand in order to study the impact of the oceans on Earth's climate and ecosystems. The day-to-day operations of these systems will become increasingly difficult if human intervention is required. In order to enable large observing systems to operate, techniques for autonomous control of assets based on science goals and data sources such as in situ measurements, remote-sensing, and model-derived data need to be developed. The Keck Institute for Space Studies (KISS) Satellites to Seafloor project works towards this goal of fully autonomous sampling [Thompson et al., 2017]. Previous ocean observing systems have relied on substantial human intervention or non-adaptive sampling strategies, including the Autonomous Ocean Sampling Networks (AOSN) [Curtin and Bellingham, 2009; Curtin et al., 1993; Haley et al., 2009; Leonard et al., 2007; Ramp et al., 2009] and the Adaptive Sampling and Prediction (ASAP) [Leonard et al., 2010] projects.

One approach is to deploy in situ assets to study coherent scientific features such as fronts, eddies, upwelling events, and harmful algal blooms. A typical strategy would be to deploy marine assets to measure transects across the feature of interest at a scale that covers the feature, as well as a baseline signal around the feature. However, asset capabilities (e.g. mobility, endurance) and prevailing ocean currents may render these science goals unachievable. Our project targets automatic generation of coordinated mission plans for teams of assets to follow these science derived observation policies (e.g. the use of multiple vehicles to perform transects orthogonal to a front). This paper specifically describes an approach using multiple vehicles to make a linear estimation of an ocean front's geometry and to continuously direct a team of marine robotic vehicles to perform orthogonal transects with the midpoint of the transect roughly centered on the target front. We describe both the general approach for front-crossing detection, front-geometry estimation, and multi-asset control as well as results from deployment and testing of this approach using short-range Iver Autonomous Underwater Vehicles in Monterey Bay in late spring 2017. The full results from the deployment, including the use of underwater gliders and Long-Range AUVs, are presented in Branch et al. [2018]. This paper focuses on the results using the Iver AUVs. This deployment was the result of a team effort between the KISS project members and the MBARI Spring 2017 CANON participants [Monterey Bay Aquarium Research Institute, 2017]. The method presented here represents significant

steps towards the fully-autonomous adaptive sampling framework as envisioned in Thompson et al. [2017].

The remainder of this paper is organized as follows. First, we provide science context to the target problem of front tracking. Second, we describe the front-crossing detection method. Third we describe the front-geometry estimation and tracking algorithm used to estimate a linear front across multiple vehicles and produce resultant vehicle transects. Fourth, we describe the experimental setup with the Iver AUVs. Fifth, we describe the results from the field deployments. Finally, we discuss related and future work and summarize the results of the experiment.

Science Context

Coherent fronts are ubiquitous features of the ocean circulation. Fronts, defined as regions of enhanced gradients in water mass or tracer properties, can occur across different scales spanning many hundreds of kilometers, such as the strong western boundary currents (e.g. the Gulf Stream), to smaller-scale filamentary features which are often associated with the fringes of coherent mesoscale eddies, but may cascade down to the meter scale [D'Asaro et al., 2017]. Due to the earth's rotation, lateral gradients in density at ocean fronts can generate strong (and strongly-sheared) along-front velocities. These velocities can, in various scenarios, act to both enhance the front by suppressing mixing or enhance mixing due to the generation of flow instabilities [Bower, Rossby, and Lillibridge, 1985]. Fronts may also be regions of intense vertical velocities and vertical fluxes. This may occur either because density surfaces tilt across strong fronts, leading to strong vertical, but still largely along-isopycnal advection. Alternatively, at sharp fronts, relative vorticity may be enhanced such that the Rossby number, defined as the ratio of the vertical relative vorticity $\zeta = \partial v/\partial x - \partial u/\partial y$ to the Coriolis frequency f, becomes comparable to or greater than 1. In this regime, the effects of rotation that constrain the velocity field to be largely horizontal begin to break down and vertical velocities can become enhanced. This dynamical regime is known as the submesocale [McWilliams, 2016; Thomas, Tandon, and Mahadevan, 2008] and can generate vertical velocities on the order of hundreds of meters per day over most of the ocean [Su et al., 2018].

This enhancement of vertical velocities at the submesoscale has important implications for the coupling between the physical circulation and ocean biogeochemistry. Primary production in the ocean is characterized by a "patchiness" implying a large degree of spatial and temporal intermittency [Martin et al., 2002]. Ocean fronts have been identified as locations where primary production may be transiently enhanced, especially in oligotrophic waters due to the injection of nutrient-rich waters to the surface ocean [Brannigan, 2016; Lévy, Klein, and Treguier, 2001; Mahadevan, 2016]. More recent work has shown that frontal instabilities can rapidly shoal the mixed layer and lead to phytoplankton blooms due to a relaxation of light limitations [Mahadevan et al., 2012; Taylor and Ferrari, 2011]. These latter studies imply that ocean fronts can also regulate carbon cycling in subpolar latitudes. Ocean fronts have also been shown to have a large impact on large marine ecosystem [Belkin, Cornillon, and Sherman, 2009].

Therefore, for both physical and biogeochemical reasons, ocean fronts tend to be hotspots of turbulent mixing, ventilation (the transfer of near-surface water properties into the ocean interior) and subduction. Furthermore, the implication is that a significant portion of the exchange between the near-surface ocean and the ocean interior occurs over a relatively small fraction of the surface ocean. Thus there is a need to dedicate greater resources to the study of these frontal features, both to improve our mechanistic understanding of how these fronts develop, evolve and impact transport properties, but also so that they can be effectively represented in data-assimilating numerical simulations of the ocean circulation.

Front-Crossing Detection

Lateral Gradient Front-Crossing Detection

The KISS team developed an algorithm to identify a subsurface oceanic fronts based on lateral gradients of a given hydrographic property. This could be temperature, buoyancy or density (if salinity data is available), or any available biogeochemical property such as dissolved oxygen or chlorophyll.

When in situ data is received in near real time, the algorithm grids the field, smooths it by applying a simple linear weighted average of immediate neighboring measured data points, and calculates the lateral gradients (Figure 1). Smoothing parameters must be selected before using this algorithm in a near real time application. The algorithm uses temporal gradients, and assumes that time can be linearly related to distance. The algorithm then calculates the lateral gradients along the transect within the layer of interest (defined beforehand by the user) as well as the mean value, and the standard deviation. The user also defines beforehand the number of standard deviations used to declare a front-crossing detection. All points above this threshold are considered potential front crossings (Figure 2). To qualify for a frontal crossing, it is required that the threshold is crossed twice (once entering and once leaving the high gradient region). Half-crossings do not qualify. The width of the front is used to choose the front crossing of interest if more than one is present. The front location, width, and time of crossing is then output for later use in vehicle tasking. An example is shown in Figure 1 and Figure 2. Time, as apposed to distance, is plotted on the x-axis as that is what the algorithm uses. Using real time data from May 4, 2017 (Figure 1d) the algorithm detects five narrow subsurface fronts from 10 to 15 m deep (Figure 2a), and selects the widest front (Figure 2d).

The front-crossing detector can be customized, for ex-

Comparison to previous methods

ample, to select only positive or negative frontal crossings. This could be useful in the event of targeting a cold or warm eddy. It can also be modified to select, instead of the widest front, the front corresponding to the maximum lateral gradient, if desired. The capability of selecting the depths over which the lateral gradients were to be evaluated allows the user to target surface fronts, or instead, focus only on deeper fronts.

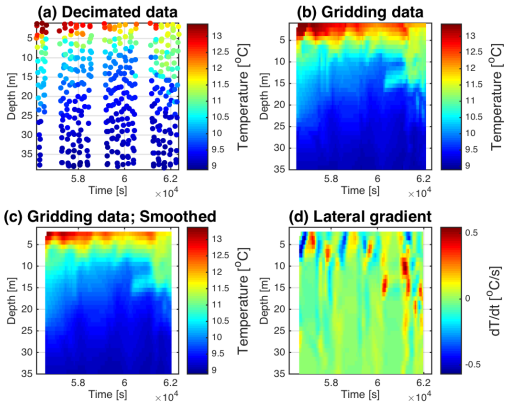

Figure 1: Lateral gradient front-crossing detector. For this example we use data obtained on May 4, 2017 from Iver 136 (segment 000). Real-time in situ temperature data (shown in scatter plot in panel a) is gridded (panel b) and smoothed (panel c). Then, lateral gradients are calculated (panel d). When used in real time, the algorithm uses temporal gradients, and assumes that time can be linearly related to distance.

Comparison to previous methods

Next we briefly compare the front-crossing detection technique presented above to a previous upwelling front detection technique developed by Monterey Bay Aquarium Research Institute (MBARI) [Zhang et al., 2012a,b, 2013]. This previous method is based on the vertical temperature structure measured on the AUV's sawtooth (i.e., yo-yo) trajectory. In stratified water, the vertical temperature difference is large: warm at surface and cold at depth. The upwelling process breaks down stratification and makes water properties more vertically homogeneous. Consequently, the vertical temperature difference between shallow and deep depths is smaller in upwelling regions. To enable an AUV to autonomously differentiate between upwelling and stratified water columns, Zhang et al. used a classification metric — the vertical temperature homogeneity index (VTHI) [Zhang et al., 2012b]

For this comparison, we use data obtained on May 1, 2017. Vertical sections in Figure 3 show the presence of a front at longitude ~122.25°W. The front separates warm, fresh water to the west, from cold, salty water to the east (Figure3a-d). The maximum lateral gradients of these properties are clearly observed at longitude

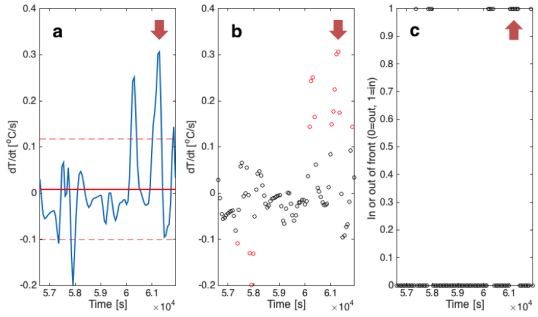

Figure 2: (Continues from Figure 1) The algorithm calculates the mean value of the lateral gradients over the layer of interest. In this example, we use data from 10m to 15m. The algorithm calculates the mean value (bold red line in panel a) and the n-standard deviation (in this case, n=1.2; red broken lines in panel a). All points above the n-value standard deviation are considered potential fronts (red circles in panel b). A boolean is used to isolate the front crossings (panel c). The width of the front is used to choose the front crossing when more than one front is present. The crossing chosen by the algorithm is marked with a red arrow.

~122.25°W (Figure3e-i). We apply the two methods described above to the upper 30 m of the water column.

The VTHI method detects a decrease of VTHI value (note that a lower VTHI value means the observed water column is more homogeneous vertically) between ~122.25-122.28°W, which corresponds to the maximum lateral gradient of buoyancy (Figure 3h). If we calculate the lateral gradient of VTHI we find agreement with the maximum lateral gradient of buoyancy (Figure 3i). Small differences are attributed to the role of salinity in the buoyancy values, which is not accounted for in VTHI.

Although both techniques give basically the same result, VTHI only captures upwelling fronts and so is specifically designed with Monterey Bay hydrography/circulation in mind. Our algorithm would be more general for detecting fronts throughout the ocean. We acknowledge that the need for interpolation in the lateral gradient method presented in this paper may pose difficulties for the implementation of this method onboard underwater vehicles. In the future, an onboard method of calculating lateral gradients without interpolation would be required.

Autonomous Control of Underwater Vehicles for Front Tracking

A technique was developed to control a group of vehicle to repeatedly sample across a dynamic ocean as it evolves over time. Vehicles must be able to modify their transects in order to adapt to the changing ocean conditions. The control algorithm (Algorithm

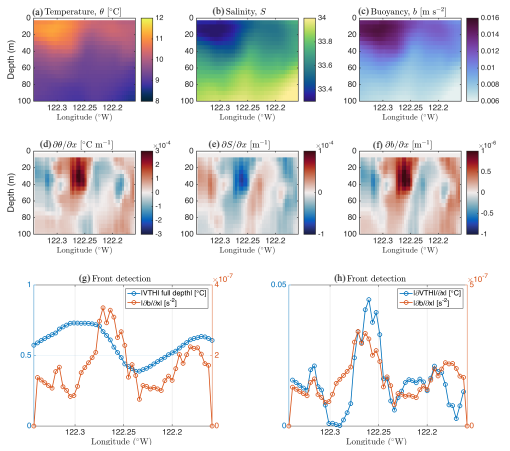

Figure 3: Comparison between lateral gradient detection method and vertical temperature homogeneity index (VTHI). (a-c) Vertical sections of (a) Temperature, θ, (b) Salinity, S, and (c) Buoyancy, b. (d-f) Lateral gradients of θ, S and b. (g) Front detection using absolute values of VTHI (blue) and lateral gradient of b (red). (h) Front detection using lateral gradients of VTHI (blue) and lateral gradient of b (red).

1) operates as follows. When first deployed, an initial estimated front location and orientation is manually provided based on available data from other assets. The vehicles are equally spaced along this estimated front. Each vehicle is commanded on an initial transect orthogonal to the provided estimated front. When the vehicle surfaces to plan, Algorithm 1 is executed. The vehicle location and the scientific data from the current transect are provided as $vehicle\_location$ and $transect\_data$ respectively. The vehicles location along the transect is calculated as $location_p$ by projecting the vehicles current location onto the commanded transect. If the vehicle has traveled a minimum distance along the commanded transect, specified by $transect\_dist_{min}$, then the front-crossing detection algorithm is run on the data from this transect. The resulting front-crossing is defined as $new\_front\_crossing$. If the vehicle is a specified distance past this new front detection, then the front is re-estimated using linear regression on front detections from all vehicles, otherwise the transect is continued. When re-estimating, only certain front detections from each vehicle are considered, specified by $valid\_front\_detections$. We used two methods when selecting the subset of detections used in the linear regression: a time based approach where detections from the last N hours were considered and a latest detection approach where only the last detection from each vehicle was considered. These two approaches are defined in the procedure $get\_estimation\_crossings$. The new $transect_p$ is calculated such that it is orthogonal to $estimated\_front$. The vehicle is then commanded on this new transect. In order to prevent the vehicle from leaving the study area, $transect\_dist_{max}$ is defined. If a transect has reached this length the front is re-estimated, a transect orthogonal to this is defined, and the vehicle is commanded on this new transect.

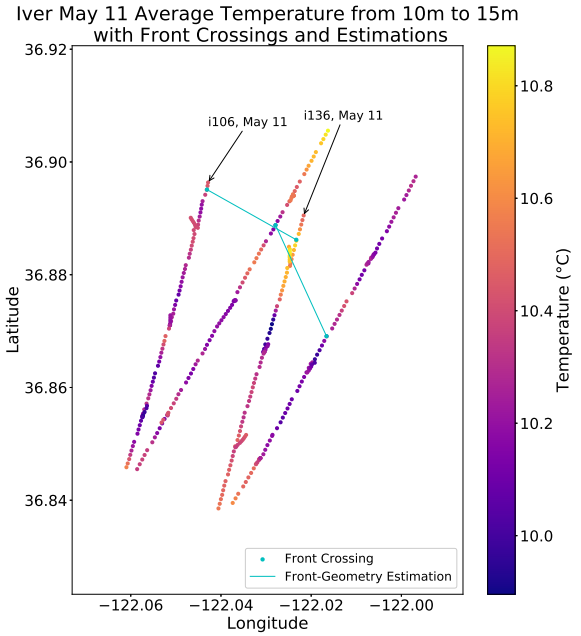

Figure 4: Iver transects on May 11 with temperature averaged from 10 meters to 15 meters plotted. Front crossings are shown as blue dots and estimated fronts are shown as blue lines. Each vehicle starting location is labeled with the vehicle name and the date. The second transect for each vehicle is orthogonal to the estimated front from the front crossings on the first transect.

Pilot Experiment

Experiment Site

The pilot experiment took place in Monterey Bay, California (36.80°N, 121.90°W) from May to June 2017.

The circulation in Monterey Bay is characterized by a persistent coastal upwelling, in response to prevalent northerly winds, which generates highly-productive cold coastal regions [Hickey, 1979; Lynn and Simpson, 1987]. Physical–biological coupling at the edges of mesoscale eddies, and turbidity plumes resulting from the interaction of the flow with topography, influence the phytoplankton ecology [Ryan, Chavez, and Bellingham, 2005]. Offshore (>150 km), the California Current (CC) flows southward with surface speeds of ∼0.25 m s^{-1} [Hickey, 1979; Lynn and Simpson, 1987]. Near the coast (<150 km), the surface flow varies seasonally, flowing northward in fall and winter [Reid and Schwartzlose, 1962], and receiving the name of the Inshore

Algorithm 1 Linear Front Delineation and Tracking

procedure VEHICLE_RETASKING($vehicle\_location$, $transect\_data$) ▷ Run this procedure when a vehicle surfaces to plan
  $location_p \leftarrow project\,(transect, vehicle\_location)$
  if $dist\left(transect\_start, location_p\right) >= transect\_dist_{min}$ **then**
    $new\_crossing \leftarrow detect\_crossings\,(transect\_data)$
    if $new\_crossing$ was detected **then**
      $crossings \leftarrow crossings \bigcup \{new\_crossing\}$
      $valid\_crossings \leftarrow get\_estimation\_crossings(crossings)$
      $estimated\_front \leftarrow linear\_regression\,(valid\_crossings)$
      $location_f \leftarrow project\,(transect, new\_front\_crossing)$
      if $dist\left(location_p, location_f\right) > \varepsilon_{past\_front}$ km **then**
        Calculate $transect_p$ **s.t.** $transect_p \perp estimated\_front$
        Command vehicle on $transect_p$
      else
        Continue on current transect
  else if $dist\left(transect\_start, location_p\right) <= transect\_dist_{max}$ **then**
    $valid\_crossings \leftarrow get\_estimation\_crossings(crossings)$
    $estimated\_front \leftarrow linear\_regression\,(valid\_crossings)$
    Calculate $transect_p$ **s.t.** $transect_p \perp estimated\_front$
    Command vehicle on $transect_p$

procedure GET_ESTIMATION_CROSSINGS($crossings$) ▷ First of two options for this procedure
  return Latest front crossing for each vehicle.

procedure GET_ESTIMATION_CROSSINGS($crossings$) ▷ Second of two options for this procedure
  return $\{crossing \in crossings \mid crossing.time > current\_time - \varepsilon_{time}\}$

Countercurrent (IC) [Lynn and Simpson, 1987]. The IC is intermittent in space and time. Below, the subsurface California Undercurrent (CU) flows northward. South of Monterey Bay, at Point Sur (36.31°N, 121.90°W), the CU separates from the coast due to topographic curvature and flow inertia [Molemaker, McWilliams, and Dewar, 2015] and forms mesoscale anticyclonic eddies whose inner edge reaches the shelf break off Monterey Bay.

In May 2017, an intensive upwelling plume spread southeastward across the mouth of Monterey Bay. A fleet of AUVs were deployed to detect and track the fronts between the upwelling plume and the stratified inner bay water. Over the shelf, KISS IVERs were set to detect lateral gradients of temperature from 10m to 15m. Over the slope, temperature in the upwelling water column was remarkably homogeneous in the vertical dimension. The operations region of the Iver AUVs are shown in Figure 5.

Iver AUVs

This work was demonstrated on two OceanServer Iver2 AUVs, shown in Figure 6. The method is extensible to other platforms and indeed other domains where the vehicles are able to at least intermittently transmit collected data and receive new instructions mid-deployment. Both of the vehicles were equipped with a hull-mounted Neil Brown conductivity/temperature sensor (Ocean Sensors Inc.) which served as the primary scientific payload for this work. Additionally, one of these vehicles, Iver-106, was an Ecomapper variant equipped with a SonTek Doppler velocity log (DVL), an Ocean-Server compass for attitude estimation, a WHOI micro-modem 2 and a depth sensor. The other Iver2 vehicle, Iver-136, was similarly equipped with the WHOI

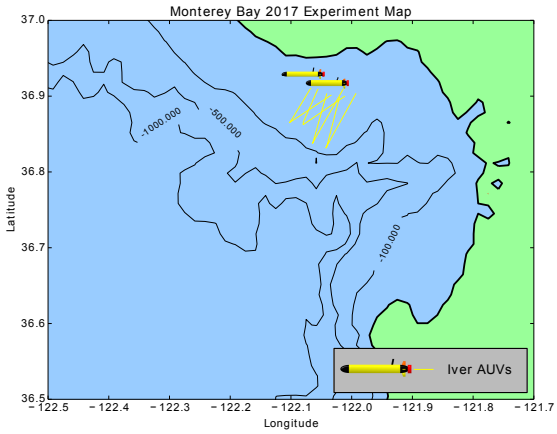

Figure 5: Map of the 2017 pilot experiment region near Monterey Bay, California. The operation region of the Iver AUVs are shown.

micro-modem 2, compass and depth sensor as well as a dual upward, downward facing 600 kHz RDI phased array DVL, a Microstrain 3DM-GX3-25 and an APS-1540 fluxgate magnetometer. The Iver2 AUVs have an approximate maximum horizontal velocity of 2 m s^{-1} and were operated at a speed of 1.5 m s^{-1} for these trials. These vehicles, are shown on board the R/V *Shana Rae* in Figure 6 during operations in August 2016.

Figure 6: OceanServer Technology, Inc. Iver2 AUVs onboard the R/V *Shana Rae*

Prior to shipping the vehicles were cross-calibrated against a Seabird SBE49 in a tank to get the relative sensor offsets. These offsets seemed to drift during shipping and the collocated measurements taken in the harbour and during deployment. In post-processing, Iver-106 was corrected for a salinity offset of 0.5180 practical salinity units.

Vehicle control

The Iver AUVs required some modifications to enable the transmission of data and receiving of new instructions during operations. Four communication modalities are available to the Iver, Iridium short burst data (SBD), Wi-Fi, 900 MHz RF, and acoustic modem. Sci-

entific data such as position, conductivity, temperature, and timestamps can be received and new commands can be sent over any of these four available communication links. Possible commands include stopping a mission, starting a mission already loaded on the vehicle, parking the vehicle and inserting segments of waypoints into the already running mission. Initially, it was planned to use the segment insertion to facilitate the retasking of the vehicles. While these commands were successfully received and interpreted by the vehicle, some unexplained behaviors while using this command precluded its ongoing use. As a temporary work around for the 2017 field trials in Monterey we used the outputs of the planning software to manually program a new mission which was then loaded onto the AUV over the RF link.

Results

We introduce a metric in order to quantify the performance of the front tracking control techniques presented here. For a given transect N, the front location, as predicted by transect $N-1$, and the front location observed on transect N are compared. As a baseline, the observed front location for transect N is also compared to the initial front-geometry estimation provided manually at the beginning of each experiment. More specifically, the metric is defined as follows. For a given transect N, define the initial front-geometry estimation manually provided at the beginning of the experiment as *initial estimation*, the front-geometry estimation used to create transect N as *predicted estimation* and the front-geometry estimation after transect N as *observed estimation*. Calculate the intersection point of transect N and the *predicted estimation* as well as the the intersection point of transect N and the *observed estimation*. The front tracking metric is defined as the distance between these two intersection points. The intersection point of transect N and *initial estimation* is also calculated. The baseline metric is defined as the distance between this intersection point and the intersection of transect N and the *observed estimation*. These two metrics are calculated for each transect. An example of the calculation for this metric can be seen in Figure 7.

The time between front crossings has an important role in the performance of this metric. Longer time between front crossings allows for a larger change in the ocean conditions. This time is a function of the speed of the vehicle and the length of a transect. The dynamism of the experiment region also affects this metric as this determines how much one might expect the front to evolve between two crossings. Due to this, direct comparisons of this metric between vehicles and operations areas are questionable, however, it can be used to assess the performance of the front tracking algorithm as well as indicate the suitability of a vehicle to a specific operating environment.

Iver AUV Results

Two Iver AUVs were operated on three days, 4 May, 9 May, and 11 May 2017. They are limited to single

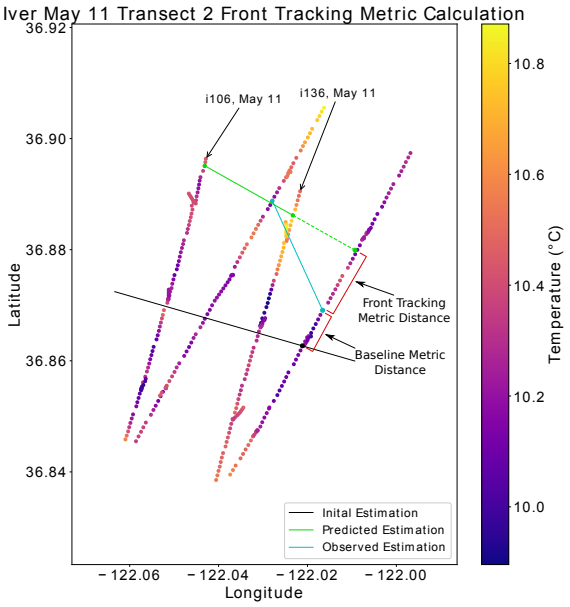

Figure 7: An example calculation of the front tracking metric. We use the May 11 i136 transect 2 for the example. The initial manually provided transect (i.e. *initial estimation*) is plotted a black line. The front-geometry estimation from the previous transect (i.e. *predicted estimation*) is plotted as a green line. The front-geometry estimation after transect 2 (i.e. *observed estimation*) is plotted as a blue line. The intersection of these three lines and the transect in question are plotted as dots of their respective colors. The distances used for the baseline and front tracking metric are shown in red.

day deployments due to the short range of the vehicles. Some operational constraints required modifications to the outlined front tracking control method. The range limitation associated with acoustic communication and the desire to have the ability for quick vehicle recovery required the two Iver AUVs to remain in close proximity to each other. The front tracking algorithm as presented does not guarantee any vehicle synchronization with regards to position. In order to solve this issue the vehicles pause at any point in which a new transect could start and waits for every other vehicle to reach their respective decision points. Once all vehicles have paused, the front-crossing detection algorithms are executed for each vehicle. If at least one vehicle has detected a front crossing, a new linear front estimation well be generated and all vehicles will be commanded orthogonal to it. If no front crossings are detected then all vehicles will continue on the current transect.

In this experiment the minimum transect distance was set at 3 km past the current estimated front. The minimum distance required for a vehicle to go past the

	Baseline Metric (m)	Front Tracking Metric (m
Average	1619.598	839.393
Std Dev	943.674	523.301

Table 1: Baseline and Front Tracking metric for the Iver Experiment on 9 and 11 May 2017

front-crossing detection on a given transect was set to 0 km, this results in the vehicle turning around at the first decision point after a front crossing is detected. The first decision point can be significantly past the detected front crossing due the minimum transect length. Ideally this would be set to a longer distance to insure that the vehicle has crossed the entire front before calculating a new transect, however due to software constraints during this deployment this was not possible. Front-geometry estimation was performed with the latest front crossing from each vehicle. The lateral gradient front-crossing detection algorithm was used with the Iver AUVs. Figure 8 shows the results of the Iver experiment on 9 and 11 May, 2017. Two transects were completed per vehicle per day. The starting locations for each vehicle on each day are labeled. Temperature averaged from 10 meters to 15 meters is plotted. All front crossing and front-geometry estimations used during the deployment are shown as blue dots and blue lines respectively. A number of different depth intervals for front-crossing detection were used during the deployment in order to examine the sensitivity of the algorithm. For reference, the front crossings and front-geometry estimations for 10 meter to 15 meter depth range are also plotted in green.

The baseline and front tracking metric for the Iver experiment is presented in Table 1. These values are calculated with the transects from both vehicles on 09 May and 11 May. We see a lower average distance with the front tracking metric compared to the baseline metric, indicating an improvement in the ability to tracking a front when using the method presented here. This result is also indicative of the suitability of the Iver platform for this specific region. Iver AUVs are fast moving vehicles with relatively short transects operating in a region where the front is mainly bathymetry driven, resulting in smaller changes in ocean conditions between front crossings. The dataset presented here is limited. It is an an initial step towards understanding the performance of the front estimation and tracking algorithm, however more data is necessary to make conclusions.

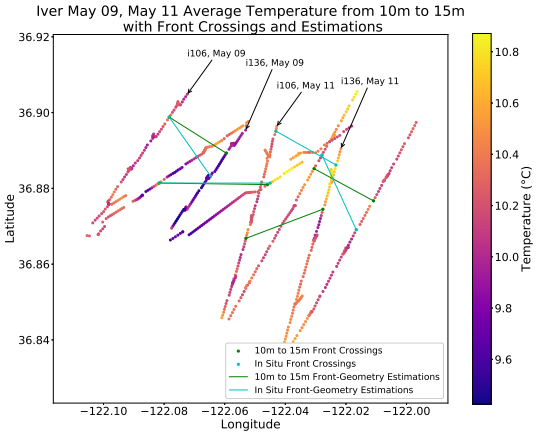

Figure 8: Map view of the temperature averaged from 10 to 15 meters for the Iver transects on 09 and 11 May, 2017. Front crossings and front-geometry estimations used during the experiment are indicated with a blue dot and blue line respectively. Front crossings and front-geometry estimations using data from 10 meters to 15 meters during the experiment are indicated with a green dot and green line respectively. The start location for each vehicle for each day is labeled.

Discussion

Related Work

Adaptive sampling and control of autonomous underwater vehicles has been extensively studied, including foundational work with the Autonomous Ocean Sampling Network [Curtin and Bellingham, 2009; Curtin et al., 1993; Haley et al., 2009; Leonard et al., 2007; Ramp et al., 2009]. Much of this work focuses on spatially adapting the control strategy in order to optimally sample a fixed region. Our method instead performs repeated focused sampling across a single front as it evolves over time.

Other work focused on control strategies that adapt to the current conditions. the Adaptive Sampling and Prediction project [Leonard et al., 2010] used adaptive control in order to coordinate 6 gliders to fly in loops at fixed spacing. Troesch et al. [2016] uses an ocean model in order to improve the station keeping ability of vertically profiling floats. Eriksen et al. [2001] describes the capabilities of a Seaglider to compensate for drift from currents using depth averaged currents over multiple dives. Those important works focus on adaptive control of vehicles based on the current conditions they are in, in order to improve sampling. We instead look at other hydrographic properties in order to optimize sampling of a specific feature.

A number of different near real-time feature tracking methods exist for applications such as thermoclines [Cruz and Matos, 2010; Sun et al., 2016; Zhang et al., 2010], and oil spills [Zhang et al., 2011]. These approaches focus on tracking a one-dimensional feature using a single vehicle, while we utilize multiple vehicles to track a two-dimensional feature. Flexas et al. [2018] uses an ocean model and autonomous planning to optimize sampling of submesoscale structures. Our approach focuses on frontal tracking using trailing in-situ vehicle data as apposed to an ocean model.

Other work has investigated two-dimensional feature tracking. Zhang et al. [2013, 2016] utilize the VTHI

front detection method on a single vehicle to detect and track an upwelling front on a zig-zag track with a fixed turn angle. Cruz and Matos [2014] tracks any gradient boundary using a single vehicle following a dynamic zig-zag pattern and a lateral gradient detection algorithm to estimate the gradient boundary using an arc whose curvature is defined by the last three front-crossing locations. Kularatne, Smith, and Hsieh [2015] tests a method in a tank to perform a zig-zag across a front using an autonomous surface vehicle. A similar method can also be applied to tracking the center of a phytoplankton bloom patch [Godin et al., 2011]. Machine learning, in the form of policy learning, has also been applied to the problem of tracking the edge of a harmful algal bloom [Magazzeni et al., 2014]. Other work focuses on tracking algal blooms by flying formations relative to the bloom as tracked by a drifter [Das et al., 2012]. Petillo, Schmidt, and Balasuriya [2012] uses a simulated network of AUVs in order to estimate the boundary of a simulated plume. These all differ from our approach in that we are using multiple vehicles in order to estimate the position and orientation of an ocean front using a method of gridded front detections as well as a linear front model.

Issues and Future Work

The front-crossing detection method is key in order for the front-geometry estimation and autonomous control portions of this method to work correctly. Throughout this experiment multiple points of improvement were identified in regards to the lateral gradient front detection. Front detection could be improved by gridding data based on distance traveled as apposed to time. This is particularly important for slower moving vehicles. The gridding process itself could also be improved by using objective mapping. In this experiment temperature was used, other ocean properties such as, buoyancy could also be used. The lateral gradient front detection method consists of many parameters, a more in-depth analysis of the effects of these parameters would be beneficial.

One of the issues encountered in the experiments was determining that the sampled front was the same as previously sampled fronts. Crossing multiple fronts would result in erroneous front-geometry estimations. In order to handle this situation our front-crossing detection technique would need to be extended in order to select a crossing based on a set of criteria such as front direction (i.e. cold-to-warm versus warm-to-cold), gradient strength, and front size. By using these different properties a specific front can be targeted.

The communication paradigms of the vehicles used is important as our technique was implemented off-board. Data decimation is an issue with vehicles that are unable to send all the available data to the planner. A data decimation scheme must be selected that allows for the front detection algorithms to perform well. These issues could be avoided by bringing the front tracking algorithm onboard the vehicles, however this introduces a number of different issues such as limited computing capabilities and inter-vehicle communication.

Conclusion

This work presents a method of adaptive control of multiple autonomous underwater vehicles in order to track an ocean front evolving over time. This method utilizes a near real-time front detection method, and an off-board planner doing front estimation using a linear model and vehicle retasking. This method builds upon the prior efforts of the AOSN deployments and takes a further step towards a fully-autonomous adaptive sampling framework [Thompson et al., 2017].

The experiment was conducted in May, 2017 in Monterey Bay, California using two short-range Iver AUVs. A front detection technique based on lateral gradients with gridded and interpolated data was used. During this experiment we demonstrated the performance of the front detection method on data from the vehicles. We also demonstrated the capability of the autonomous control method for front tracking. In doing this we introduced a metric which allows for a quantitative comparison of the front tracking algorithms performance as well as an indication of the suitability of a platform in a specific operating environment. The multi-vehicle front tracking approach allows for improved synopticity over a zig-zag method when sampling a front. While the use of off-board front detection, estimation, and retasking algorithms provided more processing power and allowed for flexible implementation for different platforms.

Acknowledgments The following work was done under the framework of the Keck Institute for Space Studies (KISS)-funded project "Science-driven Autonomous and Heterogeneous Robotic Networks: A Vision for Future Ocean Observations"[Thompson et al., 2017]. Portions of this work were funded by the Keck Institute and Woods Hole Oceanographic Institution. Portions of this work were performed by the Jet Propulsion Laboratory, California Institute of Technology, under contract with the National Aeronautics and Space Administration.

References

Belkin, I.; Cornillon, P.; and Sherman, K. 2009. Fronts in large marine ecosystems. *Prog. Oceanogr.* 81:223–236.

Bower, A.; Rossby, H. T.; and Lillibridge, J. L. 1985. The Gulf Stream–barrier or blender. *J. Phys. Oceangr.* 15:24–32.

Branch, A.; Flexas, M. M.; Claus, B.; Clark, E. B.; Thompson, A. F.; Chien, S.; Kinsey, J. C.; Fratantoni, D. M.; Zhang, Y.; Kieft, B.; Hobson, B.; and Chavez, F. P. 2018. Front delineation and tracking with multiple underwater vehicles. *J. Field Robotics* in review.

Brannigan, L. 2016. Intense submesoscale upwelling

in anticyclonic eddies. *Geophys. Res. Lett.* 43:3360–3369.

Cruz, N. A., and Matos, A. C. 2010. Adaptive sampling of thermoclines with autonomous underwater vehicles. In *OCEANS 2010*, 1–6. IEEE.

Cruz, N. A., and Matos, A. C. 2014. Autonomous tracking of a horizontal boundary. In *Oceans-St. John's, 2014*, 1–6. IEEE.

Curtin, T. B., and Bellingham, J. G. 2009. Progress toward autonomous ocean sampling networks. *Deep Sea Research Part II: Topical Studies in Oceanography* 56(3):62 – 67. AOSN II: The Science and Technology of an Autonomous Ocean Sampling Network.

Curtin, T. B.; Bellingham, J. G.; Catipovic, J.; and Webb, D. 1993. Autonomous oceanographic sampling networks. *Oceanography* 6(3):86–94.

Das, J.; Py, F.; Maughan, T.; OReilly, T.; Messié, M.; Ryan, J.; Sukhatme, G. S.; and Rajan, K. 2012. Coordinated sampling of dynamic oceanographic features with underwater vehicles and drifters. *The International Journal of Robotics Research* 31(5):626–646.

D'Asaro, E.; Shcherbina, A.; Klymak, J.; Molemaker, J.; Novelli, G.; Guigand, C.; Haza, A.; Haus, B.; Ryan, E.; Jacobs, G.; Huntley, H.; Laxague, N.; Chen, S.; F. Judt, J. W.; Barkan, R.; Kirwan, A.; Poje, A.; and Özgökmen, T. 2017. Ocean convergence an dispersion of flotsam. *Proc. Nat. Ac. Sci.* in press.

Eriksen, C. C.; Osse, T. J.; Light, R. D.; Wen, T.; Lehman, T. W.; Sabin, P. L.; Ballard, J. W.; and Chiodi, A. M. 2001. Seaglider: A long-range autonomous underwater vehicle for oceanographic research. *IEEE J. Oceanic Eng.* 26:424436.

Flexas, M. M.; Troesch, M. I.; Chien, S.; Thompson, A. F.; Chu, S.; Branch, A.; Farrara, J. D.; and Chao, Y. 2018. Autonomous sampling of ocean submesoscale fronts with ocean gliders and numerical model forecasting. *Journal of Atmospheric and Oceanic Technology* 35(3):503–521.

Godin, M. A.; Zhang, Y.; Ryan, J. P.; Hoover, T. T.; and Bellingham, J. G. 2011. Phytoplankton bloom patch center localization by the tethys autonomous underwater vehicle. In *OCEANS'11 MTS/IEEE KONA*, 1–6.

Haley, P.; Lermusiaux, P.; Robinson, A.; Leslie, W.; Logoutov, O.; Cossarini, G.; Liang, X.; Moreno, P.; Ramp, S.; Doyle, J.; Bellingham, J.; Chavez, F.; and Johnston, S. 2009. Forecasting and reanalysis in the monterey bay/california current region for the autonomous ocean sampling network-ii experiment. *Deep Sea Research Part II: Topical Studies in Oceanography* 56(3):127 – 148. AOSN II: The Science and Technology of an Autonomous Ocean Sampling Network.

Hickey, B. M. 1979. The california current system-hypotheses and facts. *Prog. Oceanogr.* 8:191–279.

Kularatne, D.; Smith, R. N.; and Hsieh, M. A. 2015. Zig-zag wanderer: Towards adaptive tracking of time-varying coherent structures in the ocean. In *2015 IEEE International Conference on Robotics and Automation (ICRA)*, 3253–3258.

Leonard, N. E.; Paley, D. A.; Lekien, F.; Sepulchre, R.; Fratantoni, D. M.; and Davis, R. E. 2007. Collective motion, sensor networks, and ocean sampling. *Proceedings of the IEEE* 95(1):48–74.

Leonard, N. E.; Paley, D. A.; Davis, R. E.; Fratantoni, D. M.; Lekien, F.; and Zhang, F. 2010. Coordinated control of an underwater glider fleet in an adaptive ocean sampling field experiment in monterey bay. *Journal of Field Robotics* 27(6):718–740.

Lévy, M.; Klein, P.; and Treguier, A.-M. 2001. Impact of sub-mesoscale physics on production and subduction of phytoplankton in an oligotrophic regime. *J. Mar. Res.* 59(4):535–565.

Lynn, R. J., and Simpson, J. J. 1987. The california current system: The seasonal variability of its physical characteristics. *J. Geophys. Res.* 92:12947–12966.

Magazzeni, D.; Py, F.; Fox, M.; Long, D.; and Rajan, K. 2014. Policy learning for autonomous feature tracking. *Autonomous Robots* 37(1):47–69.

Mahadevan, A.; D'Asaro, E.; Lee, C.; and Perry, M. J. 2012. Eddy-driven stratification initiates North Atlantic spring phytoplankton blooms. *Science* 337(6090):54–58.

Mahadevan, A. 2016. The impact of submesoscale physics on primary productivity of plankton. *Ann. Rev. Mar. Sci.* 8(17.1–17.24).

Martin, A. P.; Richards, K. J.; Bracco, A.; and Provenzale, A. 2002. Patchy productivity in the open ocean. *Global Biogeochemical Cycles* 16:1025.

McWilliams, J. C. 2016. Submesoscale currents in the ocean. *Proceedings of the Royal Society A* 472:20160117.

Molemaker, M. J.; McWilliams, J. C.; and Dewar, W. K. 2015. Submesoscale instability and generation of mesoscale anticyclones near a separation of the california undercurrent. *J. Phys. Oc.* 45:613–629.

Monterey Bay Aquarium Research Institute. 2017. Canon spring 2017 expedition.

Petillo, S.; Schmidt, H.; and Balasuriya, A. 2012. Constructing a distributed auv network for underwater plume-tracking operations. *International Journal of Distributed Sensor Networks* 2012:Article ID 191235, 12pp.

Ramp, S.; Davis, R.; Leonard, N.; Shulman, I.; Chao, Y.; Robinson, A.; Marsden, J.; Lermusiaux, P.; Fratantoni, D.; Paduan, J.; Chavez, F.; Bahr, F.; Liang, S.; Leslie, W.; and Li, Z. 2009. Preparing to

predict: The second autonomous ocean sampling network (aosn-ii) experiment in the monterey bay. *Deep Sea Research Part II: Topical Studies in Oceanography* 56(3):68 – 86. AOSN II: The Science and Technology of an Autonomous Ocean Sampling Network.

Reid, J. L., and Schwartzlose, R. A. 1962. Direct measurements of the davidson current off central california. *J. Geophys. Res.* 67:2491–2497.

Ryan, J. P.; Chavez, F. P.; and Bellingham, J. G. 2005. Physicalbiological coupling in monterey bay, california: topographic influences on phytoplankton ecology. *Mar. Ecol. Prog. Ser.* 287:23–32.

Su, Z.; Wang, J.; Klein, P.; Thompson, A. F.; and Menemenlis, D. 2018. Ocean submesoscales as a key component of the global heat budget. *Nat. Comm.* accepted.

Sun, L.; Li, Y.; Yan, S.; Wang, J.; and Chen, Z. 2016. Thermocline tracking using a portable autonomous underwater vehicle based on adaptive threshold. In *OCEANS 2016-Shanghai*, 1–4. IEEE.

Taylor, J. R., and Ferrari, R. 2011. Ocean fronts trigger high latitude phytoplankton blooms. *Geophys. Res. Lett.* 38:L23601.

Thomas, L. N.; Tandon, A.; and Mahadevan, A. 2008. Sub-mesoscale processes and dynamics. In Hecht, M. W., and Hasumi, H., eds., *Ocean Modeling in an Eddying Regime*, volume 177 of *Geophysical Monograph Series*. Washington DC: American Geophysical Union. 17–38.

Thompson, A. F.; Chao, Y.; Chien, S.; Kinsey, J.; Flexas, M. M.; Erickson, Z. K.; Farrara, J.; Fratantoni, D.; Branch, A.; Chu, S.; Troesch, M.; Claus, B.; and Kepper, J. 2017. Satellites to seafloor: Toward fully autonomous ocean sampling. *Oceanography* 30(2):160–168.

Troesch, M.; Chien, S. A.; Chao, Y.; and Farrara, J. D. 2016. Planning and control of marine floats in the presence of dynamic, uncertain currents. In *International Conference on Automated Planning and Scheduling*, 431–440.

Zhang, Y.; Bellingham, J. G.; Godin, M.; Ryan, J. P.; McEwen, R. S.; Kieft, B.; Hobson, B.; and Hoover, T. 2010. Thermocline tracking based on peak-gradient detection by an autonomous underwater vehicle. In *OCEANS 2010*, 1–4. IEEE.

Zhang, Y.; McEwen, R. S.; Ryan, J. P.; Bellingham, J. G.; Thomas, H.; Thompson, C. H.; and Rienecker, E. 2011. A peak-capture algorithm used on an autonomous underwater vehicle in the 2010 gulf of mexico oil spill response scientific survey. *Journal of Field Robotics* 28(4):484–496.

Zhang, Y.; Godin, M. A.; Bellingham, J. G.; and Ryan, J. P. 2012a. Using an autonomous underwater vehicle to track a coastal upwelling front. *IEEE Journal of Oceanic Engineering* 37(3):338–347.

Zhang, Y.; Ryan, J. P.; Bellingham, J. G.; Harvey, J. B. J.; and McEwen, R. S. 2012b. Autonomous detection and sampling of water types and fronts in a coastal upwelling system by an autonomous underwater vehicle. *Limnology and Oceanography: Methods* 10:934–951.

Zhang, Y.; Bellingham, J. G.; Ryan, J. P.; Kieft, B.; and Stanway, M. J. 2013. Two-dimensional mapping and tracking of a coastal upwelling front by an autonomous underwater vehicle. *Proc. MTS/IEEE Oceans'13* 1–4.

Zhang, Y.; Bellingham, J. G.; Ryan, J. P.; Kieft, B.; and Stanway, M. J. 2016. Autonomous four-dimensional mapping and tracking of a coastal upwelling front by an autonomous underwater vehicle. *Journal of Field Robotics* 33(1):67–81.